Materials Research. 2025; 28(suppl. 1): e20250232
DOI: https://doi.org/10.1590/1980-5373-MR-2025-0232

Electrospinning of Cellulose Acetate Propionate: Optimization of Processing Parameters for Advanced Applications

***Júlia Audrem Gomes de Oliveira Fadul*[a]*, Vitor da Silva de Souza[a], Djalma Souza[a]**

[a]*Universidade Estadual do Norte Fluminense, Campos dos Goytacazes, RJ, Brasil.*

Received: January 31, 2025; Revised: May 27, 2025; Accepted: June 8, 2025

This study investigates the electrospinning of cellulose acetate propionate (CAP) and the optimization of processing parameters to produce nanofibrous membranes with advanced functionality. CAP, a biodegradable and semi-synthetic polymer, offers exceptional thermal and mechanical properties, making it a promising material for applications in filtration, wound dressing, and containment membranes. The research systematically explores the influence of solution properties, such as polymer concentration and solvent ratios, as well as electrospinning conditions, including voltage, flow rate, and collector distance, on the morphology and uniformity of the nanofibers. Differential Scanning Calorimetry (DSC) was utilized to evaluate the thermal transitions of the material, confirming its suitability for use in applications requiring thermal stability and flexibility. The results reveal that the optimized electrospinning parameters lead to defect-free and highly uniform nanofibrous membranes, tailored for specific advanced applications. This work underscores the significance of CAP as a sustainable alternative to conventional synthetic polymers and highlights the critical role of process optimization in achieving desired material properties. The findings contribute to the growing demand for eco-friendly and high-performance materials, offering innovative solutions for industries such as healthcare and environmental remediation. This research establishes a robust foundation for further advancements in CAP-based nanotechnology.

Keywords: *Cellulose Acetate Propionate, CAP, Electrospinning, Fiber Morphology.*

Visual abstract

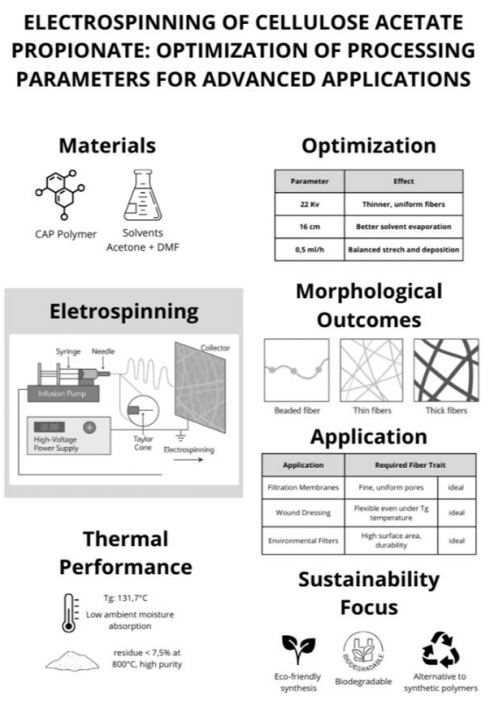

*e-mail: juliaaudrem@gmail.com
Associate Editor: Leonardo Gondim de Andrade e Silva
Editor-in-Chief: Luiz Antonio Pessan

1. Introduction

Cellulose esters are among the earliest and most widely utilized polymers, known for their thermoplastic applications. These materials exhibit a desirable combination of optical clarity, high flexural and tensile strength, impact resistance, and a high modulus[1]. One notable cellulose ester, cellulose acetate propionate (CAP), has been extensively studied due to its unique properties and broad range of applications. CAP is derived from the chemical modification of cellulose, the primary structural component of plants, in which hydroxyl groups are partially replaced by acetate and propionate groups, thereby altering its physical and chemical properties[2]. CAP is particularly valued for its excellent transparency, making it ideal for applications requiring high optical clarity, such as photographic films and optical lenses. Additionally, it demonstrates strong impact resistance, thermal stability, and chemical resistance, rendering it suitable for various industrial uses, including biomedical devices, laboratory equipment, and packaging[3-5].

The polymer's versatility extends to its compatibility with multiple processing methods, such as injection molding and extrusion, allowing it to be used across diverse sectors. CAP is also partially derived from renewable resources, providing an environmental advantage over synthetic polymers, although its biodegradability remains variable[6]. Due to its excellent mechanical properties, biocompatibility, and cost-effectiveness, CAP shows great promise for electrospinning applications[7,8].

Electrospinning is a flexible and widely used technique for fabricating polymer-based membranes with diverse applications, including filtration, tissue engineering, and energy storage[9,10]. This process involves applying a high voltage to a polymer solution, which ejects the solution from a spinneret, forming a fine fiber mat on a collector. The properties of the resultant nanofibrous membrane are heavily influenced by the selection of the polymer and its physicochemical characteristics, as well as the electrospinning parameters[11-13].

In recent years, CAP-based electrospun membranes have gained attention for their potential applications in environmental remediation and biomedical fields. Their high surface area, tunable porosity, and chemical stability make them ideal candidates for filtration systems, particularly in wastewater management, where they can effectively adsorb and remove pollutants such as synthetic dyes and heavy metals[14,15]. Furthermore, CAP's biocompatibility and mechanical strength enable its use in biomedical applications, including drug delivery systems, wound dressings, and scaffolds for tissue engineering. These diverse applications highlight the adaptability of CAP membranes in addressing both environmental and medical challenges[16-20].

Given the increasing demand for sustainable and high-performance materials, optimizing the electrospinning process for CAP membranes is crucial to enhancing their functional properties. By refining key electrospinning parameters, such as applied voltage, collector distance and flow rate it is possible to tailor the membrane's morphology and performance for specific applications. This study aims to explore the influence of these parameters on CAP membrane fabrication, with a focus on maximizing the electrospinning parameters for applications such as wastewater treatment, biomedical purpose and environmental applications.

2. Materials and Methods

2.1. Materials

The materials used in this study were: cellulose acetate propionate (CAP), supplied by Sigma-Aldrich, Brazil; acetone and dimethylformamide (DMF) supplied by Synth, Brazil.

2.2. Methods

2.2.1. Preparation of the CAP solution

Thirty milliliters of a cellulose acetate propionate (CAP) solution with a total polymer concentration of 10 wt% were prepared. A solvent mixture of acetone/DMF (75/25) was used. Initially, the polymer was mixed with acetone and stirred for 24 hours. After complete dissolution, DMF was gradually added dropwise to the polymer solution, followed by an additional 1 hour of stirring.

The viscosity of the solution was measured using a Marte MVD-8 digital viscometer, yielding a value of 419 mPa.s. The conductivity was determined with an AKSO conductivity meter, and the value obtained was 5.65 μS. These physicochemical properties are essential to achieving a stable electrospinning process and directly influence fiber morphology and formation. Appropriate viscosity ensures chain entanglement, while sufficient conductivity supports jet formation under the applied electric field.

The resulting solution was then immediately subjected to the electrospinning process.

2.2.2. Electrospinning process

Electrospinning process was carried out using a 3 mL syringe equipped with a blunt-tip metal needle in a horizontal orientation. The process was performed with an applied voltage of 22 kV to 15 kV, using a high voltage source (Faíscas ltda.) and a KdScientific ejector pump that composes the electrospinning apparatus. The temperature was maintained at 24 °C, and the humidity was kept below 35%. The polymer solution was subjected to electrospinning with a syringe pump (KdScientific ejector pump) operating at a flow rate of 0,1, 0,5 and 1 mL/h, positioned at three different distances from the collector, 16 cm, 12 cm and 10cm (Table 1 and 2). The nanofiber mats were collected on a static aluminum collector. Electrospinning was continued for 30 min for each sample per parameter.

After the electrospinning process, the nanofibrous mats were allowed to dry at room temperature for 24 h in a desiccator to ensure complete solvent evaporation. The resulting membranes were carefully removed from the collector and stored in a sealed container to prevent moisture absorption before characterization.

All electrospun membranes produced under the tested conditions exhibited similar macroscopic characteristics, regardless of the processing parameters. As shown in the representative image (Figure 1) obtained under 20 kV, 12 cm distance, and 0.5 mL/h flow rate, the membranes presented a uniform, opaque white appearance with a continuous surface and no visible defects or irregularities. The membranes were flexible, easy to handle, and maintained structural integrity

Table 1. Membrane processing parameter.

Parameters	Voltage (kV)	Distance (cm)	Flow rate (ml/h)
1	22	16	0.1
2	22	12	0.1
3	22	10	0.1
4	20	16	0.1
5	20	12	0.1
6	20	10	0.1
7	15	16	0.1
8	15	12	0.1
9	15	10	0.1
10	22	16	0.5
11	22	12	0.5
12	22	10	0.5
13	20	16	0.5
14	20	12	0.5
15	20	10	0.5
16	15	16	0.5
17	15	12	0.5
18	15	10	0.5
19	22	16	1
20	22	12	1
21	22	10	1
22	20	16	1
23	20	12	1
24	20	10	1
25	15	16	1
26	15	12	1
27	15	10	1

during removal from the collector and manipulation, as evidenced by their clean edges and intact form. Due to the lack of distinguishable visual differences between samples at the macroscopic level, only scanning electron microscopy (SEM) was used to evaluate and compare the morphological variations among the fibers.

2.2.3. Thermal characterization

The thermal properties and thermal stability of the CAP samples were investigated by differential scanning calorimetry (DSC) on a TA Instruments DSC25 Discovery. Sample was heated from -40°C to 250°C at a rate of 10°C/ min under nitrogen. It was also studied by thermogravimetric analysis (TGA) using a TA Instruments SDT650 Discovery thermogravimetric analyzer, with a temperature range between 20 and 800 °C, and a heating rate of 10 °C/ min. During the analyses, a flow of 100 ml/min of nitrogen was used to guarantee an inert atmosphere.

2.2.4. High resolution electron microscopy (SEM-FEG) analysis

Morphological studies of prepared nanofibers were conducted with a high resolution electron microscopy microscope (SEM-FEG) (MIRA 4 LMS fabricated by TESCAN) with an accelerating voltage of 10 kV. All samples were coated with gold under a fin coater for 120 seconds before observation. The average fiber diameter of the electrospun fibers was measured by ImageJ software from the SEM pictures in original magnification of 5kx and 10kx.

Table 2. Average fiber diameter according to the parameters.

Sample	Diameter (µm)	Sample	Diameter (µm)	Sample	Diameter (µm)
1	0,263±0,144	10	0,195±0,113	19	0,239±0,125
2	0,300±0,109	11	0,138±0,056	20	0,279±0,151
3	0,302±0,135	12	0,164±0,073	21	0,245±0,166
4	0,256±0,149	13	0,131±0,068	22	0,229±0,119
5	0,247±0,087	14	0,143±0,067	23	0,325±0,151
6	0,220±0,072	15	0,159±0,114	24	0,236±0,123
7	0,197±0,064	16	0,159±0,083	25	0,258±0,141
8	0,235±0,083	17	0,147±0,057	26	0,325±0,163
9	0,196±0,078	18	0,197±0,095	27	0,393±0,152

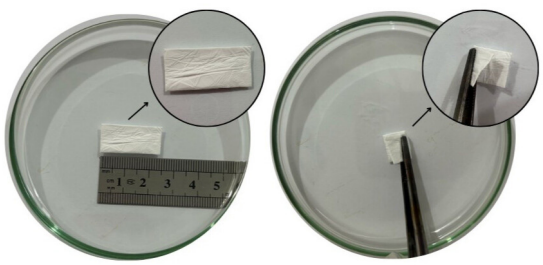

Figure 1. Macroscopic image of the CAP membrane, with parameters: 20 Kv, 12 cm and 0.5 ml/h.

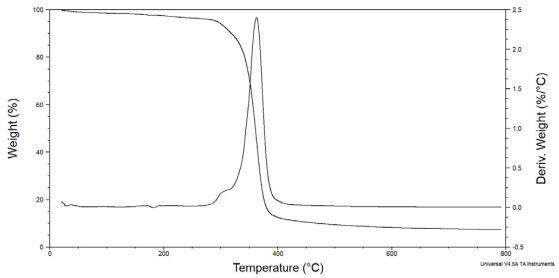

Figure 2. Thermogravimetric curve and its derivative curve (DTG) corresponding to a pure cellulose acetate propionate membrane.

3. Results and Discussion

3.1. Thermal characterization

The thermogravimetric analysis (TGA) of cellulose acetate propionate (CAP) reveals several important thermal characteristics. Initially, a small weight loss (Figure 2) of 0.112 mg (1.12%) occurs below 100°C, which can be attributed to the loss of adsorbed moisture or light volatile components. The minimal moisture absorption suggests that CAP has hydrophobic properties, which is advantageous in membrane applications, as it can enhance water selectivity while reducing the swelling and fouling of the membrane during filtration.

Between 100°C and 200°C (Figure 2), additional peaks at 92.98°C and 171.71°C are observed, with weight losses of 1.189% (0.148 mg) and 0.679% (0.067 mg), respectively. These events likely correspond to the removal of low-molecular-weight components or minor degradation of the side chains. This thermal behavior indicates that CAP maintains structural stability under moderate heat exposure, a crucial factor for membranes exposed to moderately high temperatures during cleaning or sterilization processes. The major thermal decomposition occurs at around 363.68°C, with a significant weight loss of 89.184% (8.861 mg) (Figure 2). This corresponds to the breakdown of the cellulose backbone and the acetate and propionate functional groups, marking the upper limit of CAP's thermal stability. The ability to withstand temperatures up to 300°C without significant degradation makes CAP membranes suitable for processes that involve thermal cycling or high-temperature cleaning, enhancing their durability in wastewater treatment systems[2,21,22].

A residue of 0.727 mg (7.317%) remains at 800°C (Figure 2). This residual material likely consists of inorganic fillers, char, or other thermally stable components. The low residual weight indicates CAP's high purity and minimal inorganic content, which is beneficial for ensuring consistent membrane performance and reducing potential leaching of unwanted substances into the treated water. These results demonstrate that CAP's thermal stability, low moisture absorption, and high purity make it an excellent candidate for wastewater treatment membranes. Its thermal stability up to 300°C ensures the material can endure operational and cleaning conditions, while its hydrophobic nature enhances fouling resistance and water selectivity[21-23]. Furthermore, the high purity of the material minimizes contamination risks, ensuring reliable performance over extended periods of use[22].

In the DSC thermal analysis (Figure 3) of the cellulose acetate propionate (CAP) membrane, the first heating curve (Figure 3a) reveals two well-defined endothermic peaks, while the second heating cycle exhibits a glass transition temperature (Tg). The first endothermic peak, observed at 69.44 °C with an onset temperature of 35.53 °C and an enthalpy of 6.221 J/g, can be attributed to events such as the evaporation of residual solvents, moisture removal, or initial molecular relaxation[23]. This behavior is relevant for applications sensitive to heat, such as wound dressings, where flexibility and comfort near body temperature are desirable. However, this initial transition also highlights a thermal limitation that may affect performance under higher temperature conditions. The second endothermic peak, occurring at 186.52 °C with an onset temperature of 167.77 °C and an enthalpy of 9.593 J/g, suggests a more significant thermal event, such as partial melting or the onset of thermal degradation. This indicates that the membrane exhibits good thermal stability, making it suitable for applications requiring moderate temperature resistance, such as filtration membranes, oil/water separation membranes, and dental barrier membranes. The thermal resistance up to this range also supports its use in industrial processes and sterilization conditions[24-27].

In the second heating cycle (Figure 3b), the glass transition temperature (Tg) was observed at 131.70 °C, marking the temperature at which the material transitions from a rigid to a more flexible state. This relatively high Tg is advantageous for applications requiring dimensional stability and mechanical resistance, such as filtration membranes and dental barrier membranes. Despite the relatively high glass transition temperature (Tg), the film still exhibits adequate flexibility, which is advantageous for wound dressing applications. Nevertheless, further enhancements—such as the incorporation of plasticizers—could improve comfort and adaptability at body temperature[22,27-29].

These characteristics underline the potential of CAP membranes in various fields, with opportunities for specific modifications to better meet the requirements of each application.

3.2. Effect of voltage

As observed in the literature, the shape of the initial droplet at the needle tip tends to change with the increase

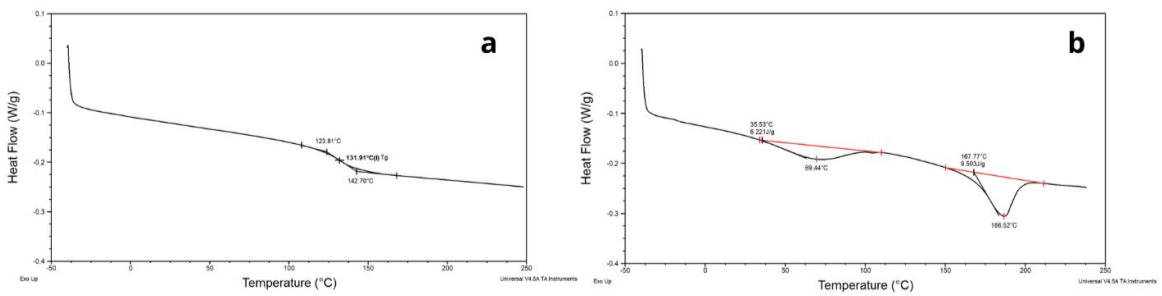

Figure 3. DSC analysis corresponding to: a) first heating curve; b) second heating curve of a pure cellulose acetate propionate membrane.

in applied voltage. That said, the applied voltage is also strongly correlated with bead formation in the fibers[28-31]. Bead formation primarily occurs due to the high electric field applied to the system. The morphology of the electrospun fibers shifts from a defect-free structure to a beaded structure as the electric field strength increases[28,32]. Fiber diameter gradually decreases with the increasing applied electric field, as demonstrated in Table 2. To investigate the effect of voltage on the membrane structure and fiber diameter of cellulose acetate propionate (CAP), electrospinning was performed under electric potentials ranging from 15 to 22 kV, while other parameters were kept constant (solution concentration of 10% w/v in the CAP/acetone/DMF system, a feed rate of 0,1, 0,5, 1 ml/h, and a needle-to-collector distance of 16 cm). The voltage range was selected based on the premise that the lowest voltage should be slightly above the critical voltage required for Taylor cone formation.

Different morphological appearances of the electrospun membranes were observed under various applied voltages, as indicated by SEM images (Figure 4, 5 and 6). The experimental results indicate that reducing the applied voltage decreases bead density and leads to the formation of uniform fibers (Figure 4, 5 and 6). The formation of smaller-diameter nanofibers with an increase in applied voltage is attributed to the stretching of the polymer solution, as there is greater charge repulsion within the jet. Nevertheless, increasing the applied voltage beyond a critical value will result in the formation of beads or nanofibers. The formation of beads with an increase in applied voltage is attributed to the reduction in the size of the Taylor cone and the increase in jet velocity[31].

In Figure 4 at 22 kV and a tip-to-collector distance of 16 cm, the fibers exhibited uniform morphology with minimal bead formation. This condition produced the smallest average fiber diameter and the narrowest diameter distribution, attributed to the strong electric field and extended flight time, which promoted efficient jet stretching and solvent evaporation. Reducing the tip-to-collector distance to 12 cm at the same voltage resulted in slightly increased bead formation, a larger average fiber diameter, and a broader diameter distribution, likely due to reduced stabilization time for the polymer jet. At 10 cm, the fibers showed more prominent bead formation and further increased diameters, reflecting limited jet elongation and solvent evaporation. At 20 kV, the fibers produced at a 16 cm distance displayed moderate uniformity, with some bead formation and slightly larger average diameters compared to 22 kV. The diameter distribution was broader, indicating reduced stretching forces. At 12 cm, bead formation and diameter variation increased, while the fibers at 10 cm showed significant bead formation and a broader diameter distribution, demonstrating the limitations of shorter flight times and reduced stretching. At 15 kV, fibers electrospun at 16 cm exhibited irregular morphology with prominent bead formation. The average diameter was the largest among all tested voltages, and the diameter distribution was broad, reflecting insufficient electrostatic forces for effective jet stretching. Reducing the distance to 12 cm resulted in further increases in bead formation and diameter variability, while at 10 cm, the fibers displayed extensive bead formation, the largest diameters, and the broadest distribution.

At a reduced flow rate of 0.5 mL/h (Figure 5), the fiber morphology and diameter distribution improved due to enhanced jet stretching and solvent evaporation. At 22 kV and 12 cm, fibers exhibited the smallest diameters and the most uniform distribution, with minimal bead formation. Shorter distances (12 cm and 10 cm) resulted in slightly larger diameters and more beads, though the lower flow rate mitigated these effects compared to higher flow rates. At 20 kV, fibers showed moderate uniformity, with smaller diameters and fewer beads at 10 cm, while shorter distances led to increased variability. At 15 kV, the reduced flow rate improved fiber uniformity across all distances but still resulted in the largest diameters and bead formation due to insufficient stretching forces.

Increasing the voltage with a flow rate of 1 mL/h significantly influenced the fiber diameter distribution (Figure 6). At 22 kV, the higher voltage combined with the flow rate produced thinner fibers and narrower diameter distributions at a 16 cm distance due to enhanced stretching forces. However, reducing the distance to 12 cm and 10 cm resulted in broader distributions and more bead formation, caused by limited stabilization time and reduced jet elongation. At 20 kV, fibers were slightly thicker with moderate uniformity at 10 cm, but bigger distances led to increased bead formation and broader distributions, as the stretching forces were weaker compared to 22 kV. At 15 kV, the lowest voltage produced the thickest fibers and the broadest diameter distributions across all distances, reflecting inadequate electrostatic forces to counteract the increased flow rate.

Electrospun fibers with optimized morphology and diameter distribution have diverse applications based on the parameters used during production. Fibers produced at 22 kV with a 16 cm tip-to-collector distance, exhibiting uniform morphology, minimal bead formation, and small diameters, are suitable for filtration membranes, where fine pores and consistent fiber diameter are essential for efficient particle capture[33-36]. Conditions resulting in moderate bead formation, such as 20 kV at 12 cm, may be applied in scaffolds for tissue engineering, as bead-like structures can mimic the porosity required for cell attachment and proliferation[37]. Fibers with prominent bead formation and larger diameters, like those at 15 kV and 10 cm, are better suited for applications requiring high porosity, such as sound absorption materials[38,39].

Reducing the flow rate to 0.5 mL/h enhances fiber uniformity, making these fibers ideal for drug delivery systems, where controlled release depends on precise fiber morphology[40]. These trends align with observations by Chinnappan et al.[40], who reported that optimal fiber morphology is achieved within specific ranges of voltage and tip-to-collector distance, typically around 13–15 cm, which balances stretching and drying time.

Moreover, as highlighted by Ben Dassi and Chamam[41], optimized electrospun membranes have proven critical in wastewater treatment applications due to their high surface area, chemical resistance, and tunable morphology. Fibers produced under 22 kV with 16 cm spacing showed

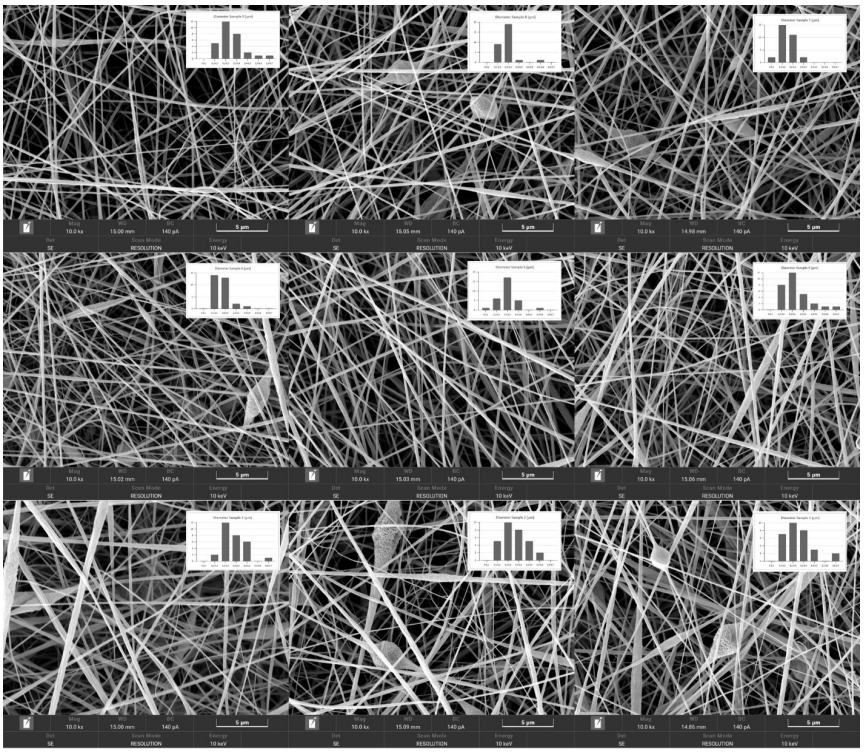

Figure 4. SEM images showing the applied voltage effect on the morphology of the CAP fibers electrospun from a 10% w/v CAP/acetone/DMF solution, with a feeding rate of 0.1 ml/h, at a tip-to-collector distance of 10, 12 and 16 cm and varied electrical potentials of 22, 20 e 15kV.

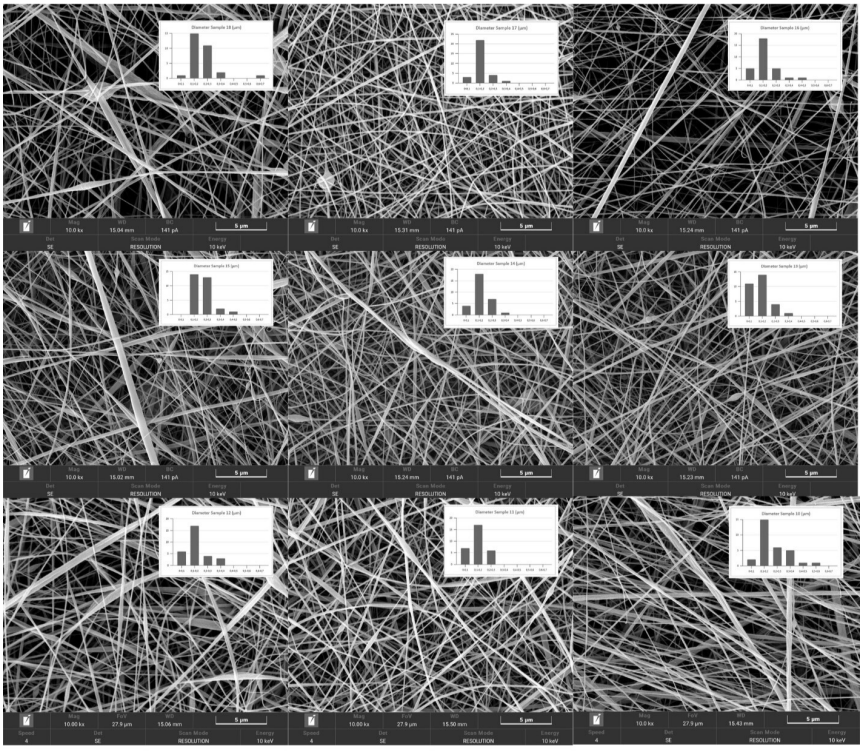

Figure 5. SEM images showing the applied voltage effect on the morphology of the CAP fibers electrospun from a 10% w/v CAP/acetone/DMF solution, with a feeding rate of 0.5 ml/h, at a tip-to-collector distance of 10, 12 and 16 cm and varied electrical potentials of 22, 20 e 15kV.

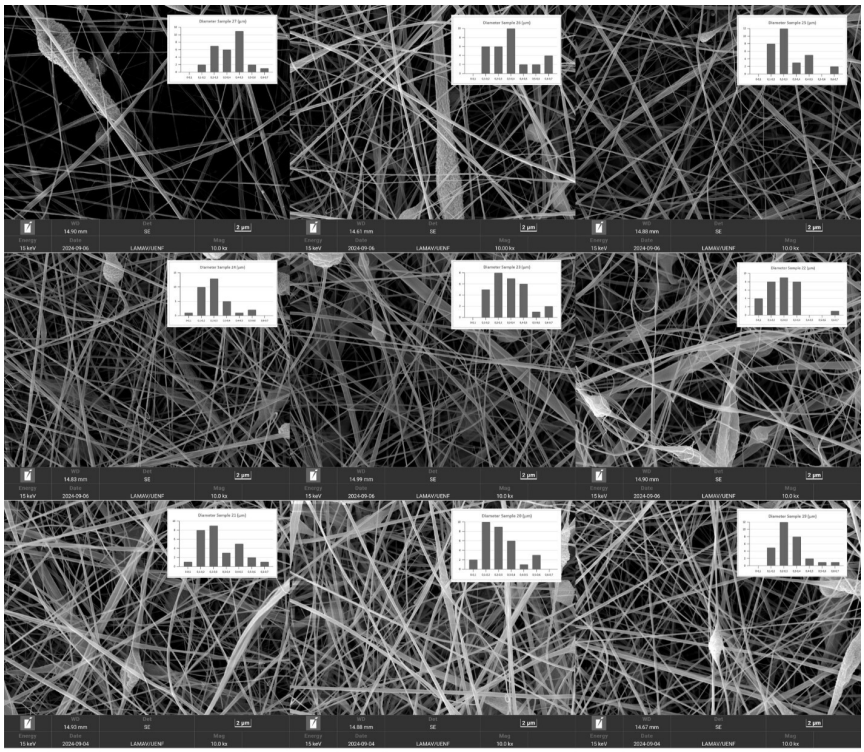

Figure 6. SEM images showing the applied voltage effect on the morphology of the CAP fibers electrospun from a 10% w/v CAP/acetone/DMF solution, with a feeding rate of 1 ml/h, at a tip-to-collector distance of 10, 12 and 16 cm and varied electrical potentials of 22, 20 e 15kV.

excellent potential for such uses, offering uniformity and fine diameters ideal for efficient pollutant capture in filtration systems. Conversely, increasing the flow rate to 1 mL/h and using 22 kV with 16 cm produces thinner fibers with narrow diameter distributions, suitable for applications in protective clothing due to their improved mechanical properties and breathability[42-44].

3.2. Effect of the needle tip to collecting device distance

The distance between the needle and the collector plays a critical role in determining the shape and size of electrospun fibers. It influences key factors such as deposition time, solvent evaporation rate, and jet stability, requiring an optimal distance to ensure fibers dry properly before reaching the collector. This parameter is closely related to the polymer solution concentration and applied voltage[45,46].

The SEM images provided illustrate the effect of varying the needle tip-to-collector distance (10 cm, 12 cm, and 16 cm) and flow rate (0.1 ml/h, 0.5 ml/h, and 1 ml/h) (Figure 7, 8, 9) on the morphology of electrospun fibers, with a constant applied voltage of 22 kV.

At a short distance (10 cm), the limited flight time restricts solvent evaporation, resulting in non-uniform fibers and bead formation, particularly at higher flow rates. For instance, at a low flow rate (0.1 ml/h, Figure 7,3), the fibers appear relatively uniform, but increasing the flow rate to 0.5 ml/h (Figure 7,12) leads to thicker fibers and imperfections. At the highest flow rate (1 ml/h, Figure 7, number 21), bead defects are prominent, as the polymer solution does not have sufficient time to stretch and solidify. For the intermediate distance (12 cm), the slightly longer flight time provides a better balance between solvent evaporation and fiber stretching. At a low flow rate (0.1 ml/h, Figure 7,2), fibers are uniform and bead-free. Increasing the flow rate to 0.5 ml/h (Figure 7,11) produces slightly thicker fibers with fewer defects compared to the 10 cm distance. However, at the highest flow rate (1 ml/h, Figure 7,20), defects such as beads and inconsistent fiber deposition begin to emerge due to the excessive volume of polymer solution. At the longest distance (16 cm), the extended flight time allows for sufficient solvent evaporation and jet stretching, resulting in the most uniform fibers, especially at low flow rates. For example, at 0.1 ml/h (Figure 7,1), the fibers are thin, uniform, and bead-free. At a medium flow rate (0.5 ml/h, Figure 5,10), the fibers remain consistent but slightly thicker. However, at the highest flow rate (1 ml/h, Figure 6,19), defects such as beads and uneven deposition are observed, as the high flow overwhelms the evaporation and stretching process.

At 16 cm, represented by samples 6 and 15 (Figure 8), the fibers are smooth, uniform, and bead-free, showcasing the benefits of extended flight time. The increased distance provides sufficient time for solvent evaporation, resulting in well-formed fibers with consistent diameters. Among these, sample 24 shows a random fiber distribution with many beads, very thick fibers and thin fibers that can be

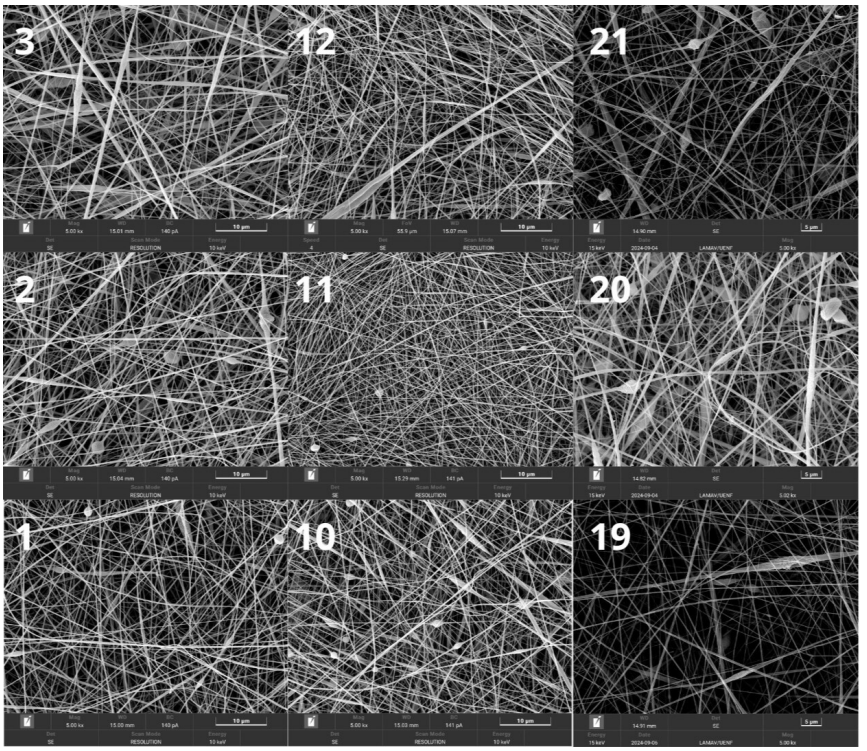

Figure 7. Morphology of the CAP mats (5000x) for the samples obtained for a 10% (w/v) polymer solution, a 75/25 acetone/DMF solvent solution and at a traveling according to the parameters in Table 1 and 2, determined by the following numbers: 1, 2, 3; 10, 11, 12; 19, 20, 21.

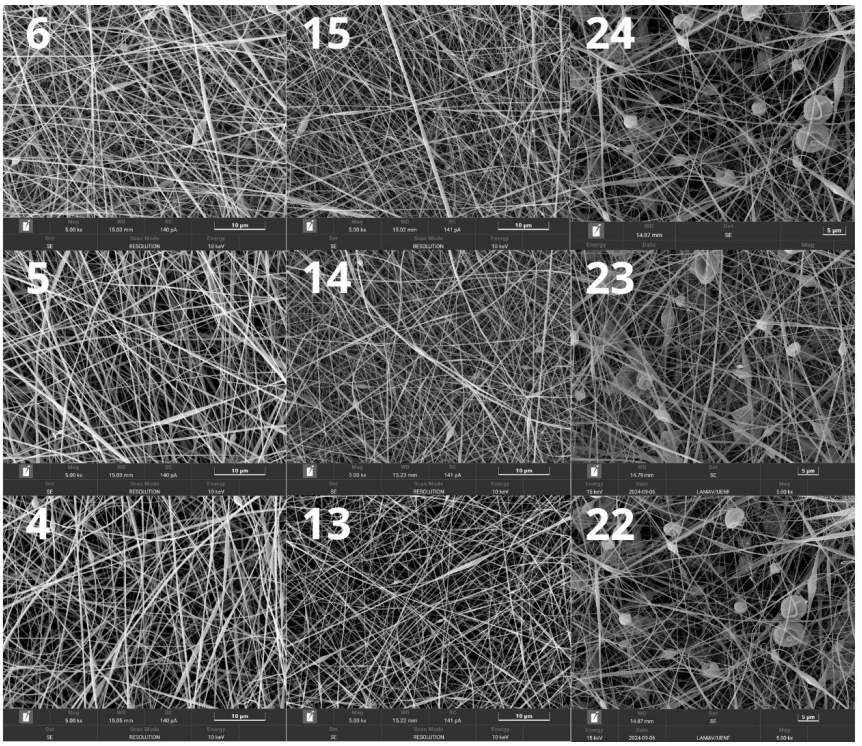

Figure 8. Morphology of the CAP mats (5000x) for the samples obtained for a 10% (w/v) polymer solution, a 75/25 acetone/DMF solvent solution and at a traveling according to the parameters in Table 1 and 2, determined by the following numbers: 4, 5, 6; 15, 14, 13; 24, 23, 22.

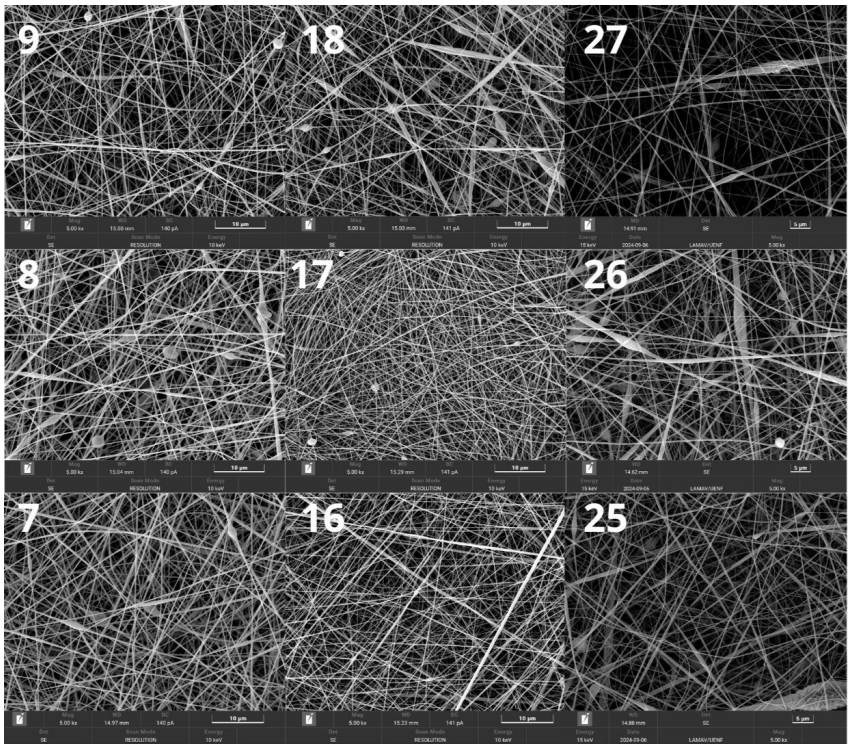

Figure 9. Morphology of the CAP mats (5000x) for the samples obtained for a 10% (w/v) polymer solution, a 75/25 acetone/DMF solvent solution and at a traveling according to the parameters in Table 1 and 2, determined by the following numbers: 7, 8, 9; 16, 17, 8; 25, 26, 27.

related to the increase in flow rate. The prolonged drying time at 16 cm, at 6 and 15, minimizes bead formation, making these fibers suitable for high-precision applications. At 12 cm, observed in samples 5 and 14 (Figure 8), the fibers remain mostly uniform but show slight variations in diameter compared to those at 16 cm. The shorter distance increases the electric field strength, promoting better jet stretching but slightly reducing the time available for complete solvent evaporation. Sample 14 shows a lot of defects and thin fibers. The samples 5 and 12 indicate that 12 cm offers a good balance between productivity and fiber quality. However, slight thickening of the fibers is visible in comparison to those produced at 16 cm. At 10 cm, as seen in sample 22, fiber morphology becomes less consistent, with noticeable bead formation and increased fiber diameters. The reduced needle-to-collector distance and the increase of the flow rate shortens the flight time, hindering solvent evaporation and leading to rapid deposition of the polymer solution. Sample 22, as observed in 24 and 23, exhibits significant bead formation, indicative of instability in the jet and incomplete drying. The irregular fiber structure at this distance demonstrates the limitations of shorter needle-to-collector distances, especially under high flow rates and voltages. On the other hand, images 4 and 13 show a uniform structure with homogeneous fiber diameters, indicating good interlocking, an essential characteristic for membranes used in filtration processes[47,48].

At 16 cm, corresponding to samples 7, 16, and 25 (Figure 9), the fibers exhibit a smooth, uniform, and bead-free morphology. The increased distance allows for extended flight time, enabling sufficient solvent evaporation and improved jet stability. This configuration produces fine fibers with minimal defects, ideal for applications requiring precision and uniformity. However, sample 25 (1 ml/h) shows beads and other fibers with a thicker diameter and fibers with a very thin diameter, as shown in Table 2 (e.g. 0.258±0.141), where a greater standard deviation can be observed as a result of the heterogeneous diameter distribution. This phenomenon can be explained by the higher flow rate. At 12 cm, as observed in samples 8, 17, and 26 (Figure 9), the fibers maintain a high degree of uniformity but begin to show slight variations in diameter compared to those at 16 cm. The reduced distance intensifies the electric field strength, promoting enhanced jet stretching but offering slightly less time for solvent evaporation. Sample 26, for example, produces fibers that are thicker than those at 16 cm but remain uniform, with some bead defects. This intermediate distance strikes a balance between fiber consistency and production efficiency, making it suitable for applications where moderate quality and higher throughput are desired. At 10 cm, represented by samples 9, 18, and 27 (Figure 9), the fibers display noticeable irregularities, including increased diameter and bead formation. The strong electric field and short flight time hinder complete solvent evaporation, leading to the rapid deposition of the polymer

solution. Sample 27, in particular, exhibits thicker fibers with significant bead formation, likely due to jet instability and insufficient drying. While shorter distances may increase production rates, the compromised fiber quality limits their suitability for high-precision applications.

The comparative analysis of these distances reveals a clear progression in fiber morphology. At 16 cm, the fibers are thin, uniform, and bead-free, reflecting the optimal conditions for jet stabilization and solvent evaporation. At 12 cm, the fibers remain consistent with slight increases in diameter, providing a good trade-off between quality and productivity. At 10 cm, the fibers are thicker and more irregular, with notable bead formation, demonstrating the limitations of reduced drying time and stronger electric fields.

The interplay of other parameters, such as voltage and flow rate, further influences the observed trends. Higher voltages increase jet stretching, counteracting the thickening effects of shorter distances to some extent. However, excessively high voltages at shorter distances often destabilize the jet, exacerbating bead formation. Lower flow rates improve fiber uniformity by reducing droplet size and enabling better solvent evaporation, even at shorter distances. In contrast, higher flow rates contribute to defect formation, particularly at 10 cm, due to rapid deposition and incomplete drying. Longer distances (16 cm) produce fine, uniform fibers suitable for applications like tissue engineering and filtration. Intermediate distances (12 cm) balance fiber quality and productivity, while shorter distances (10 cm) increase throughput but compromise fiber uniformity. By optimizing the needle-to-collector distance in conjunction with voltage and flow rate, the electrospinning process can be tailored to meet specific application requirements[47-49].

3.3. The effect of flow rate on fiber diameter in correlation with voltage and distance

The flow rate, in combination with voltage and needle-to-collector distance, significantly affects the fiber diameter and morphology during the electrospinning process. The statistical analysis of fiber diameters, measured from SEM images (magnification 10,000X) across varying flow rates (Figure 4-9), demonstrated that flow rate alone does not significantly affect fiber diameter. However, variations in flow rate can interact with voltage and distance to impact fiber morphology and uniformity.

At lower flow rates (e.g., 0.1 mL/h), a smaller volume of polymer solution is ejected, leading to smaller droplet sizes and a more stable Taylor cone. This allows the electric field, especially at higher voltages (e.g., 22 kV), to sufficiently stretch the polymer jet, resulting in thinner fibers. Additionally, longer needle-to-collector distances (e.g., 16 cm) provide more time for solvent evaporation, which enhances fiber uniformity and minimizes defects.

Conversely, increasing the flow rate (e.g., 1 mL/h) introduces a higher volume of solution at the needle tip, forming larger droplets and potentially destabilizing the Taylor cone. Under these conditions, the electric field strength may become insufficient to fully stretch the polymer jet, especially at shorter distances (e.g., 10 cm). This can lead to the formation of beads, unspun droplets, and fibers with wider diameter distributions. At very high flow rates, the increased volume also reduces solvent evaporation time, resulting in flattened or web-like structures on the collector[16]. The optimal flow rate (e.g., 0.5 mL/h) balances the solution ejection rate with the electric field strength, maintaining a stable Taylor cone and producing uniform fibers with narrow diameter distributions. This balance is particularly evident when paired with moderate voltages and distances (e.g., 20 kV and 12 cm), which allow for sufficient stretching and solvent evaporation[49-52]. Very high or very low flow rates can lead to the formation of defects in the Taylor cone, where the jet can split in two, generating a random diameter distribution (Figure 10). Sometimes the diameters are too thick, sometimes too thin. The fiber can even break during the deposition of the collector[51-54].

Morphological analysis revealed that inappropriate flow rates—either too high or too low—result in defects such as blobs, splitting, or branched fibers. These defects arise due to insufficient stretching at high flow rates or due to shear stress and intermittent jet formation at low flow rates. The combination of optimized flow rate, voltage, and needle-to-collector distance is crucial for achieving high-quality fibers suitable for advanced applications.

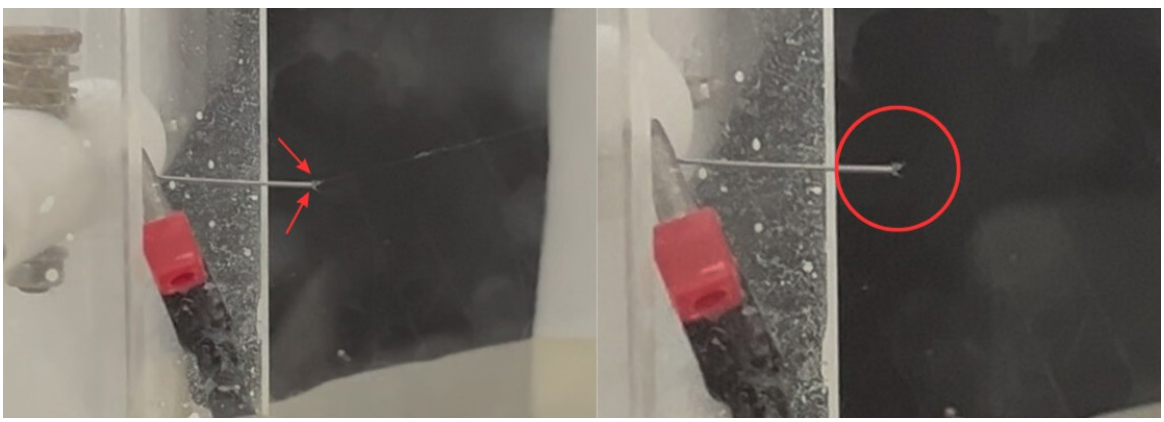

Figure 10. Taylor cone defects during the electrospinning process.

4. Conclusion

This study demonstrates the potential of cellulose acetate propionate (CAP) as a versatile and sustainable polymer for the development of nanofibrous membranes using electrospinning.

The study revealed that applied voltage played a pivotal role in shaping fiber morphology. At higher voltages (15-22 kV), thinner fibers were produced due to enhanced electrostatic stretching. However, excessively high voltages caused droplet formation and disrupted fiber uniformity. Similarly, collector distance significantly influenced fiber properties. Shorter distances (10-16 cm) generated thinner, more uniform fibers, but extremely short distances led to random deposition and clumping. Flow rate was another key factor; higher rates resulted in thicker fibers due to reduced stretching time before solidification and increased process instability. These findings highlighted the intricate interplay of voltage, collector distance, and flow rate. Lower voltages and shorter distances produced thicker, more defective fibers, while higher voltages combined with longer distances yielded thinner, more uniform fibers. The results emphasized the necessity of optimizing electrospinning parameters to fabricate CAP fibers with desirable properties for diverse applications.

By systematically optimizing processing parameters, we achieved defect-free membranes with superior morphological uniformity and tailored properties for advanced applications. The analysis of thermal transitions using DSC revealed that CAP membranes possess the necessary thermal stability and flexibility, making them highly suitable for applications in filtration, wound dressing, and containment systems.

The significance of this research lies in its alignment with the global push toward sustainable and biodegradable materials, offering a viable alternative to synthetic polymers commonly used in various industries. CAP's biodegradability and compatibility with advanced fabrication techniques like electrospinning position it as a key material for addressing current environmental and technological challenges. Furthermore, this study emphasizes the importance of optimizing electrospinning parameters to control fiber morphology and enhance material performance. The insights gained from this research provide a solid framework for future studies aimed at expanding the applicability of CAP-based nanofibrous membranes in diverse fields, including environmental protection and healthcare. The findings also highlight the role of innovation in material science in driving sustainable development and creating impactful technological solutions.

5. Acknowledgement

The authors would like to thank CAPES and FAPERJ for their financial support, and Márcio Toledo Barreto for the administrative support.

6. References

1. Buchanan CM, Gedon SC, White AW, Wood MD. Cellulose acetate propionate and poly(tetramethylene glutarate) blends. Macromolecules. 1993;26(11):2963-7. http://doi.org/10.1021/ma00063a048.
2. Schilling M, Bouchard M, Khanjian H, Learner T, Phenix A, Rivenc R. Application of chemical and thermal analysis methods for studying cellulose ester plastics. Acc Chem Res. 2010;43(6):888-96. http://doi.org/10.1021/ar1000132. PMid:20455567.
3. Kim J, Chen Y, Kang KS, Park YB, Schwartz M. Magnetic field effect for cellulose nanofiber alignment. J Appl Phys. 2008;104(9):096104. http://doi.org/10.1063/1.3006140.
4. Abdellah Ali SF, William LA, Fadl EA. Cellulose acetate, cellulose acetate propionate and cellulose acetate butyrate membranes for water desalination applications. Cellulose. 2020;27(16):9525-43. http://doi.org/10.1007/s10570-020-03434-w.
5. Huang K, Wang B, Cao Y, Li H, Wang J, Lin W, et al. Homogeneous preparation of Cellulose Acetate Propionate (CAP) and Cellulose Acetate Butyrate (CAB) from sugarcane bagasse cellulose in ionic liquid. J Agric Food Chem. 2011;59(10):5376-81. http://doi.org/10.1021/jf104881f. PMid:21452895.
6. Martín-Alfonso MA, Rubio-Valle JF, Hinestroza JP, Martín-Alfonso JE, Franco JM. Environmentally friendly tailor-made oleo-dispersions of electrospun cellulose acetate propionate nanostructures in castor oil for lubricant applications. Nano Materials Science. 2024;7(1):90-104. http://doi.org/10.1016/j.nanoms.2024.02.003.
7. Gao C, Li X, Song C, Wei G, Zhao X, Wang S, et al. Electrospun polyimide/cellulose acetate propionate nanofiber membrane-based gel polymer electrolyte with fast lithium-ion transport and high interface stability for lithium metal batteries. Cellulose. 2023;30(14):9113-26. http://doi.org/10.1007/s10570-023-05434-y.
8. Kim TY, Mi Y. Fabrication of porous cellulose acetate propionate/polybutylene succinate microfibers by high speed centrifugal spinning. Text Color Finish. 2023;35(4):239-45.
9. Haider A, Haider S, Kang IK. A comprehensive review summarizing the effect of electrospinning parameters and potential applications of nanofibers in biomedical and biotechnology. Arab J Chem. 2018;11(8):1165-88. http://doi.org/10.1016/j.arabjc.2015.11.015.
10. Chen H, Huang M, Liu Y, Meng L, Ma M. Functionalized electrospun nanofiber membranes for water treatment: a review. Sci Total Environ. 2020;739:139944. http://doi.org/10.1016/j.scitotenv.2020.139944. PMid:32535464.
11. Akram MW, Hoque MMU, Miah MS, Shahid MA, Hossain MF, Mahmud SH. Fabrication and characterization of antimicrobial wound dressing nanofibrous materials by PVA-betel leaf extract. Heliyon. 2023;9(7):e17961. http://doi.org/10.1016/j.heliyon.2023.e17961. PMid:37483766.
12. Yu D, Wang M, Ge R. Strategies for sustained drug release from electrospun multi-layer nanostructures. Wiley Interdiscip Rev Nanomed Nanobiotechnol. 2022;14(3):e1772. http://doi.org/10.1002/wnan.1772. PMid:34964277.
13. Kerwald J, Moura CF Jr, Freitas ED, Moraes JDP II, Vieira RS, Beppu MM. Cellulose-based electrospun nanofibers: a review. Cellulose. 2021;29(1):25-54. http://doi.org/10.1007/s10570-021-04303-w.
14. Ponnusamy R, Kumaravel V, Nachimuthu S. Synthesis of cellulose acetate, cellulose propionate and cellulose butyrate for the removal of synthetic dyes. AIP Conf Proc. 2022;2659:100037. http://doi.org/10.1063/5.0109788.
15. Soylak M, Unsal YE, Aydin A, Kizil N. Membrane filtration of nickel(II) on cellulose acetate filters for its preconcentration, separation, and flame atomic absorption spectrometric determination. Clean. 2010;38(1):91-5. http://doi.org/10.1002/clen.200900189.
16. Li X, Wang KY, Helmer B, Chung TS. Thin-film composite membranes and formation mechanism of thin-film layers on hydrophilic cellulose acetate propionate substrates for forward osmosis processes. Ind Eng Chem Res. 2012;51(30):10039-50. http://doi.org/10.1021/ie2027052.

17. Sobral MCCM, Sobral AJFN, Guthrie JT, Gil MH. Ketotifen controlled release from cellulose acetate propionate and cellulose acetate butyrate membranes. J Mater Sci Mater Med. 2008;19(2):677-82. http://doi.org/10.1007/s10856-007-0168-4. PMid:17619990.
18. Bifari EN, Khan SB, Alamry KA, Asiri AM, Akhtar K. Cellulose acetate based nanocomposites for biomedical applications: a review. Curr Pharm Des. 2016;22(20):3007-19. http://doi.org/10.2174/1381612822666160316160016. PMid:26979093.
19. Vatanpour V, Pasaoglu ME, Barzegar H, Teber OO, Kaya R, Bastug M, et al. Cellulose acetate in fabrication of polymeric membranes: a review. Chemosphere. 2022;295:133914. http://doi.org/10.1016/j.chemosphere.2022.133914. PMid:35149008.
20. Khan MD, Singh A, Khan MZ, Tabraiz S, Sheikh J. Current perspectives, recent advancements, and efficiencies of various dye-containing wastewater treatment technologies. J Water Process Eng. 2023;53:103579. http://doi.org/10.1016/j.jwpe.2023.103579.
21. Islam MD, Uddin FJ, Rashid TU, Shahruzzaman M. Cellulose acetate-based membrane for wastewater treatment: a state-of-the-art review. Mater Adv. 2023;4(18):4054-102. http://doi.org/10.1039/D3MA00255A.
22. Souza D, Castillo TE, Rodríguez RJS. Effects of hydroxyvalerate contents in thermal degradation kinetic of cellulose acetate propionate/poly(3-hydroxyalkanoates) blends. J Therm Anal Calorim. 2012;109(3):1353-64. http://doi.org/10.1007/s10973-011-2152-y.
23. Edgar KJ, Buchanan CM, Debenham JS, Rundquist PA, Seiler BD, Shelton MC, et al. Advanced in cellulose ester performance and application. Prog Polym Sci. 2001;26(9):1605-88. http://doi.org/10.1016/S0079-6700(01)00027-2.
24. Kargarzadeh H, Huang J, Lin N, Ahmad I, Mariano M, Dufresne A, et al. Recent developments in nanocellulose-based biodegradable polymers, thermoplastic polymers, and porous nanocomposites. Prog Polym Sci. 2018;87:197-227. http://doi.org/10.1016/j.progpolymsci.2018.07.008.
25. Freitas RRM, Senna AM, Botaro VR. Influence of degree of substitution on thermal dynamic mechanical and physicochemical properties of cellulose acetate. Ind Crops Prod. 2017;109:452-8. http://doi.org/10.1016/j.indcrop.2017.08.062.
26. Anulaya SV, Subash A, Gholap V, Kandasubramanian B. Electrospinning of cellulose acetate for methylene blue dye removal. Hybrid Advances. 2024;6:100205. http://doi.org/10.1016/j.hybadv.2024.100205.
27. Mohamed A, Hassabo A. Modified cellulose acetate membrane for industrial water purification. Egypt J Chem. 2022;65(131):53-70. http://doi.org/10.21608/ejchem.2022.147513.6393.
28. Chinnappan BA, Krishnaswamy M, Bal T, Rajora AD. In vitro-in vivo wound healing efficacy of *Tridax procumbens* extract loaded carboxymethylcellulose film. Int J Biol Macromol. 2023;253(Pt 1):126695. http://doi.org/10.1016/j.ijbiomac.2023.126695. PMid:37673143.
29. Ayyanar CB, Bal T, Fahaduddin, Sharma S, Gayathri B, Rinusuba V, et al. *In-vitro* and *in-vivo* investigation of wound healing efficacy of *Syzygium cumini* leaf extracts loaded carboxymethylcellulose film. Int J Biol Macromol. 2024;275(Pt 2):133691. http://doi.org/10.1016/j.ijbiomac.2024.133691. PMid:38972647.
30. Liu X, Lin T, Gao Y, Xu Z, Huang C, Yao G, et al. Antimicrobial electrospun nanofibers of cellulose acetate and polyester urethane composite for wound dressing. J Biomed Mater Res B Appl Biomater. 2012;100(6):1556-65. http://doi.org/10.1002/jbm.b.32724. PMid:22692845.
31. Samadian H, Salehi M, Farzamfar S, Vaez A, Ehterami A, Sahrapeyma H, et al. In vitro and in vivo evaluation of electrospun cellulose acetate/gelatin/hydroxyapatite nanocomposite mats for wound dressing applications. Artif Cells Nanomed Biotechnol. 2018;46(Suppl 1):964-74. http://doi.org/10.1080/21691401.2018.1439842. PMid:29458271.
32. Zong X, Kim K, Fang D, Ran S, Hsiao BS, Chu B. Structure and process relationship of electrospun bioabsorbable nanofiber membranes. Polymer. 2002;43(16):4403-12. http://doi.org/10.1016/S0032-3861(02)00275-6.
33. Christoforou T, Doumanidis C. Biodegradable cellulose acetate nanofiber fabrication via electrospinning. J Nanosci Nanotechnol. 2010;10(9):6226-33. http://doi.org/10.1166/jnn.2010.2577. PMid:21133179.
34. Mousavi SM, Nejad ZM, Hashemi SA, Salari M, Gholami A, Ramakrishna S, et al. Bioactive agent-loaded electrospun nanofiber membranes for accelerating healing process: a review. Membranes. 2021;11(9):702. http://doi.org/10.3390/membranes11090702. PMid:34564519.
35. Al-Attabi R, Dumée LF, Schütz JA, Morsi Y. Pore engineering towards highly efficient electrospun nanofibrous membranes for aerosol particle removal. Sci Total Environ. 2018;625:706-15. http://doi.org/10.1016/j.scitotenv.2017.12.342. PMid:29306158.
36. Yang Y, Cao X, Lin J. Implantation of web-like cellulose nanofibrils on electrospun fibrous membrane for boosting filtration performance. Int J Biol Macromol. 2025;288:138686. http://doi.org/10.1016/j.ijbiomac.2024.138686. PMid:39672409.
37. Nicosia A, Keppler T, Müller FA, Vazquez B, Ravegnani F, Monticelli P, et al. Cellulose acetate nanofiber electrospun on nylon substrate as novel composite matrix for efficient, heat-resistant, air filters. Chem Eng Sci. 2016;153:284-94. http://doi.org/10.1016/j.ces.2016.07.017.
38. Liu H, Zhu Y, Zhang C, Zhou Y, Yu DG. Electrospun nanofiber as building blocks for high-performance air filter: a review. Nano Today. 2024;55:102161. http://doi.org/10.1016/j.nantod.2024.102161.
39. Jonidi Shariatzadeh F, Currie S, Logsetty S, Spiwak R, Liu S. Enhancing wound healing and minimizing scarring: a comprehensive review of nanofiber technology in wound dressings. Prog Mater Sci. 2025;147:101350-0. http://doi.org/10.1016/j.pmatsci.2024.101350.
40. Chinnappan BA, Krishnaswamy M, Xu H, Hoque ME. Electrospinning of biomedical nanofibers/nanomembranes: effects of process parameters. Polymers. 2022;14(18):3719. http://doi.org/10.3390/polym14183719. PMid:36145868.
41. Ben Dassi R, Chamam B. Nanomaterial-enhanced membranes for advanced water and wastewater treatment: a comprehensive review. Rev Environ Sci Biotechnol. 2025;24(2):477-511. http://doi.org/10.1007/s11157-025-09723-9.
42. Fahanwi AN, Yasir M, Nguyen HT, Saha N, Saha T, Sedlařík V, et al. In situ polyaniline polymerization on electrospun cellulose acetate nanofibers derived from recycled waste filter butts of cigarettes for the enhanced removal of methyl orange and rhodamine. Chem Eng Res Des. 2023;201:18-30. http://doi.org/10.1016/j.cherd.2023.11.043.
43. Mo J, Hu D, Liu X, Sun Y, Li X, Wang C, et al. Eco-friendly ZIF-67/rice straw-derived cellulose acetate electrospun nanofiber mats for efficient CO2 capturing and selectivity removal of methyl orange dye. J Environ Chem Eng. 2022;10(6):108989. http://doi.org/10.1016/j.jece.2022.108989.
44. Pillay V, Dott C, Choonara YE, Tyagi C, Tomar L, Kumar P, et al. A review of the effect of processing variables on the fabrication of electrospun nanofibers for drug delivery applications. J Nanomater. 2013;2013(1):1-22. http://doi.org/10.1155/2013/789289.
45. Filimon A, Serbezeanu D, Rusu D, Bargan A, Lupa L. Design of high-performance electrospun membranes for protective clothing applications. Membranes. 2024;14(11):244. http://doi.org/10.3390/membranes14110244. PMid:39590630.
46. Gorji M, Jeddi AA, Gharehaghaji AA. Fabrication and characterization of polyurethane electrospun nanofiber membranes for protective clothing applications. J Appl Polym Sci. 2012;125(5):4135-41. http://doi.org/10.1002/app.36611.

47. Megelski S, Stephens JS, Chase DB, Rabolt JF. Micro- and nanostructured surface morphology on electrospun polymer fibers. Macromolecules. 2002;35(22):8456-66. http://doi.org/10.1021/ma020444a.
48. HMTShirazi R, Mohammadi T, Asadi AA, Tofighy MA. Electrospun nanofiber affinity membranes for water treatment applications: a review. J Water Process Eng. 2022;47:102795. http://doi.org/10.1016/j.jwpe.2022.102795.
49. Nasir AM, Awang N, Jaafar J, Ismail AF, Othman MHD, Rahman MA, et al. Recent progress on fabrication and application of electrospun nanofibrous photocatalytic membranes for wastewater treatment: a review. J Water Process Eng. 2021;40:101878. http://doi.org/10.1016/j.jwpe.2020.101878.
50. Escribá A, Silva BATT, Lourenço SA, Cava CE. Incorporation of nanomaterials on the electrospun membrane process with potential use in water treatment. Colloids Surf A Physicochem Eng Asp. 2021;624:126775. http://doi.org/10.1016/j.colsurfa.2021.126775.
51. Uddin Z, Ahmad F, Ullan T, Nawab Y, Ahmad S, Azam F, et al. Recent trends in water purification using electrospun nanofibrous membranes. Int J Environ Sci Technol. 2021;19(9):9149-76. http://doi.org/10.1007/s13762-021-03603-9.
52. Elaissaoui I, Sayeb S, Ounif I, Ferhi M, Karima H, Ennigrou DJ. Preparation and characterization of acetate cellulose electrospun nanofibers membrane: potential application on wastewater treatment. Heliyon. 2024;10(12):e32552. http://doi.org/10.1016/j.heliyon.2024.e32552. PMid:39183835.
53. Ding B, Li C, Hotta Y, Kim J, Kuwaki O, Shiratori S. Conversion of an electrospun nanofibrous cellulose acetate mat from a super-hydrophilic to super-hydrophobic surface. Nanotechnology. 2006;17(17):4332-9. http://doi.org/10.1088/0957-4484/17/17/009.
54. Lee H, Nishino M, Sohn D, Lee JS, Kim IS. Control of the morphology of cellulose acetate nanofibers via electrospinning. Cellulose. 2018;25(5):2829-37. http://doi.org/10.1007/s10570-018-1744-0.

Data Availability

The authors confirm that the data supporting the findings of this study are available within the article and are also available from the corresponding author, upon reasonable request.